

Numerical Computation of Fission-Product Poisoning Build-up and Burn-up Rate in a Finite Cylindrical Nuclear Reactor Core

Mathew Ademola Jayeola^{1*}, Musbaudeen Kewulere Fasasi²,
Adebimpe Amos Amosun¹, Ayodeji Olalekan Salau³, Babatunde Michael Ojo¹

Abstract: All fission products are classified as reactor poisons because they absorb neutrons to some extent, most of which buildup slowly as the fuel burns up and eventually constitutes a long term reactivity effect in the core. Amidst the numerous fission fragments produced per fission, the presence of Xenon-135 and Samarium-149 has the greatest effect on a reactor core multiplication factor because of their large absorption cross-sections. In this study, we present a modified one-group time independent neutron diffusion equation using the method of Eigen functions and also provided an algorithm to calculate the temperature variations of the neutron fluxes. The solution obtained from the diffusion equation was used to determine the initial thermal neutron flux needed for the reactor startup. The four basic fission-product poisoning buildup and burn-up rate equations were solved using direct integration method and constant flux approximation over a particular time interval. Furthermore, a computer algorithm called Java code for Fission-Product Poisoning Build-up and Burn-up (Jac-FPPB) code was designed to calculate the temperature variations of the neutron fluxes, fission - isotopes cross sections and the atom concentrations of the fission products over a given time interval. The result from Jac-FPPB code show that the neutron fluxes and neutron energies increase as the temperature of the fuel increases. In addition, the computed atom concentrations of each fission isotopes at any given time interval show that the isotopes increasingly build up steadily at the initial time interval and rises to a constant level where the buildup rate of the isotopes approximately equals its burn up rate. This study concluded that the designed algorithm (JaC-FPBB code) proved efficient as it could compute the build-up and burn-up rates for the two important fission fragments in a nuclear reactor core. The code is easily accessible and can serve as a tool for the development of nuclear energy in developing countries, especially Nigeria.

Keywords: Numerical computation, Cylindrical reactor core, Fission-Products poisoning, Neutron diffusion equation, Samarium-149 and Xenon-135

1. Introduction

All nuclear reactors operate on the principle of nuclear fission (Marcum and Spinrad, 2013). This is the process in which a heavy atomic nucleus splits into two smaller fragments (Fermi, 1940). The fission fragments are in very excited states and they emit neutrons, other subatomic particles, and photons. The emitted neutrons may then cause new fissions which in turn yield more neutrons, and so forth. Such self-sustaining series of fissions

constitutes a fission chain reaction. In addition, as the fission chain reaction continues, many fission fragments popularly called nuclear reactor poisons buildup in the reactor core. However, some of these poisonings particularly Xenon-135 and Samarium-149 have large absorption cross sections for thermal neutrons, thereby constituting significant threat to the normal operation of the reactor system.

The remainder of this paper is organized as follows. The related work done is presented in Section 2.

¹Obafemi Awolowo University, Faculty of Science, Department of Physics and Engineering Physics, Ile-Ife, Nigeria.

²Obafemi Awolowo University, Center for Energy Research and Development, Ile-Ife, Nigeria.

³Obafemi Awolowo University, Faculty of Technology, Department of Electronic and Electrical Engineering, Ile-Ife, Nigeria.

*Corresponding author: senatormao6@gmail.com

Citation: Jayeola, M.A., Fasasi, M.K., Amosun, A.A., Salau, A.O., Ojo, B.M. (2018). Numerical Computation of Fission-Product Poisoning Build-up and Burn-up Rate in a Finite Cylindrical Nuclear Reactor Core. *Bilge International Journal of Science and Technology Research*. 2(1), 17-30.

Section 3 explains our proposed method in detail. Section 4 presents and discusses the results, and the paper is finally concluded in section 5.

2. Related Works

In recent years, several studies related to the numerical computation of poison build-up and burn-up in the core of a cylindrical nuclear reactor as well as the general computer codes to solving these equations were carried out but were not made accessible to people inside or outside the scientific communities where they were developed. Fission isotopes buildup/burnup and fuel depletion codes have been developed and used in the nuclear industry since the introduction of digital computing. Codes used today to calculate fission product buildup and burnup as well as their reactivity transient effects include coupled neutronics calculation and fission poisoning formation codes and post-processing modules.

Yesilyurt et al. (2011) developed a multi-physics code system called Oak Ridge Isotope Generation and Depletion Scale (ORIGEN-S). This code solves a set of ordinary differential equations to compute the time dependent quantity of nuclides that vary due to radioactive decay, isotopic transmutation, and nuclear fission. In ORIGEN-S, nuclide number densities at a given time, t , decay constants, monoenergetic microscopic cross sections and neutron flux were all computed and incorporated into the code. The neutron flux does vary with time, due to changes in the spectrum and isotopic concentrations. Advanced depletion code systems like ORIGEN-S generally involve coupling between lattice physics transport methods that solve for the neutron flux spectrum and generate problem-dependent cross sections and depletion methods that simulate the time-dependent isotopic evolution. Whether this is done in one integrated code or as several modular codes, the functional requirements are largely the same: neutron transport (or diffusion) codes generate accurate problem-dependent cross sections for use in the depletion calculation, and the nuclide concentrations from the depletion calculation are applied in the transport (or diffusion) calculation in order to reflect the time-dependent composition changes associated with irradiation.

Meanwhile, earlier in 1998, ORIGEN-S program was first developed by the Chemical Technology Division of Oak-ridge national laboratory (ORNL) to provides reliable bench mark result for such

computation which includes multi-group neutron diffusion calculations, fuel burnup analysis and fission product poisoning buildup and burnup calculations. The numerical methods used in ORIGEN SCALE or ORIGEN-S (Hermann and Wesfall, 1998) solve for arbitrary matrix element coupling using a hybrid approach that combines the matrix exponential method with Bateman equations for short-lived nuclides to obtain stable numerical solutions for all nuclides. The method allows for cyclical transition feedback, eliminating the need of analytical methods to use linearized chains. However, the highest fidelity approach simply uses neutron absorption and fission reaction information and fissile material cross sections generated in the code to determine the nuclide concentration at the next time step. This type of model allows for all of the neutron flux information to be integrated into the calculation without post-processing and additional manipulation of the neutron flux and cross-sections of fissile materials. Fission isotope's absorption and fission cross sections data for individual nuclides are available as output for Monte Carlo codes like Monte Carlo N-Particle (MCNP), (Briesmeister, 1993). The major requirement is that some sets of energy-dependent cross-sections are made available for each nuclide of interest at the required material temperature. The neutronics code is used to calculate core criticality (k_{eff}) and the energy dependent neutron flux for a reactor or a region within the reactor. Typical neutronics code such as MCNP Code uses the neutron flux information and power density to compute the fission nuclides composition for the different time step. The process is repeated for an extensive duration of fuel burnup cycle. Usually a one-group thermal neutron flux generation code is used to perform the fission buildup and burnup analysis. Typical depletion/fission-product generation codes include ORIGEN (Kord and Lulu, 2012) and EPRI-CINDER (England et al., 1976).

Parma, (2002) presented a Fortran computer code design. This design was used to aid the analysis, prediction, and optimization of fuel burnup performance in a nuclear reactor. This computer program is called BURNCAL- A Nuclear Reactor Burnup Code Using MCNP Tallies. The code uses output parameters generated by the Monte Carlo neutronics code MCNP to determine the isotopic inventory as a function of time and power density. BURNCAL was also designed to study the reactivity effects and isotopic inventory as a function of time for a nuclear reactor system. Neutron transmutation, fission and radioactive

decay are included in the modeling of the production and removal terms for each isotope of interest. For a fueled region, neutron transmutation, fuel depletion, fission-product poisoning, actinide generation, burnable poison loading and depletion effects are included in the calculation. In addition, its flexibility feature makes it useful in fission product poisoning calculation. Furthermore, BURNCAL uses the neutron absorption and fission information generated from the neutronics code in calculating the nuclide mixture for the next time step of interest.

Arshad (1994) presented a study on Xenon and Samarium's behavior in a typical PARR-1 core comprising 22 low enriched uranium (LEU) fuel elements operating at 5MW and 10MW using a point model. In the point model, the core power is represented by average thermal flux. For this purpose, the flux-power correlation was taken from the core calculation results and the fuel parameters were taken from the lattice studies carried out in the context of conversion and upgradation of PARR- 1.

In another model called cell model, Xenon concentration is evaluated using the actual fission density and flux values which were obtained from cell calculations. Using this methodology and employing the parameters of low enriched uranium (LEU) core, the equilibrium Xenon and post-shutdown Xenon effects were studied. The analysis also pointed out that equilibrium xenon reactivities were also evaluated using cell model and 3-dimensional core model. The core calculations were carried out with the help of a developed computer code called FCAP. The result indicated that when the core is fresh or the reactor has been in a shutdown state for a few days, the amount of xenon in the core is zero. After reactor start-up the concentration of Xe-135 starts increasing immediately. In contrast with Sm-149 it attains the equilibrium value rather quickly.

Hence, this study considered the buildup and burnup rate of the aforementioned fission-product poisonings in a cylindrical nuclear reactor core with

the aim of laying a computational foundation for the calculation of the corresponding reactivity poisoning effects that may be introduced due to the presence of the two fission products in an operating reactor.

3. Methods and Approximations Used

The solution to the steady state neutron diffusion equation with appropriate boundary conditions is presented in this section. Furthermore, the analytical solution to the four (4) fission rate equations were solved.

3.1. Neutron flux

The production and consumption of these isotopes (Xenon-135 and Samarium-149) depend on the neutron flux in the reactor and its operation history. Any change in the neutron flux which occurs during reactor start-up or shut down, is accompanied by a corresponding change in the concentration of these isotopes. Therefore, it is important to recall that the basic processes governing the behavior of the core of a nuclear reactor include variations in the distribution of neutrons in the reactor core. Neutron flux is a measure of the combined effect of the motions of neutrons. The description of the neutron distribution is based on the neutron transport equation. This equation is a linear form of the Boltzmann equation used in the study of gases. The analytical solution of the Boltzmann equation cannot be obtained as a result of its complexities which includes the presence of too many independent variables, complicated energy variations of microscopic cross-sections and complex geometrical structure of the core materials.

Hence for simplicity, an approximation of the transport equation known as the multi-group neutron diffusion equation is best used for reactor calculations in order to obtain reasonably accurate results. The multigroup time-independent neutron diffusion equation can be written as Eq. (1) (Larmash, 1966):

$$D_g \nabla^2 \Phi_g - \Sigma_{ag} \Phi_g - \sum_{h=g+1}^N \Sigma_{g \rightarrow h} \Phi_h + \sum_{h=1}^{g-1} \Sigma_{h \rightarrow g} \Phi_h = -S_g \quad (1)$$

Describing Eq. (1), we have:

$D_g \nabla^2 \Phi_g$ is the diffusion term in group g.

where D_g is the diffusion coefficient of the neutron flux in group g and Φ_g is the neutron flux of energy group g .

Also, $\Sigma_{ag}\Phi_g$ is the absorption rate in group g , $\Sigma_{h=g+1}^N \Sigma_{g \rightarrow h} \Phi_g$ is the total rate at which neutrons scatter out of g^{th} group into h^{th} group, $\Sigma_{h=1}^{g-1} \Sigma_{h \rightarrow g} \Phi_g$ is the transfer rate into g^{th} group from h^{th} group.

Lastly, S_g is the total neutrons emitted into the groups from the sources.

However, a modified one-group time-dependent neutron diffusion equation is presented and is sufficient to describe the behavior of the thermal neutron flux present in the reactor core and this is considered the starting point for fission product-poisoning formation. The group transfer terms in the multi-group equation will be omitted, so that the rate at which neutrons are produced and absorbed is given as:

$$D\nabla^2\phi(\vec{r}, t) - \Sigma_a\phi(\vec{r}, t) + S(\vec{r}, t) = \frac{1}{v} \frac{\partial\phi(\vec{r}, t)}{\partial t} \quad (2)$$

Here, ϕ is the one-group flux, D and Σ_a are the one-group diffusion coefficient and macroscopic absorption cross-section for the fuel-coolant mixture, S is the source density (i.e. the number of neutrons emitted per cm^3/sec), and v is the

neutron speed. The modified one-group neutron diffusion equation is obtained by making the derivative term to be equal to zero so that it is properly termed steady-state neutron diffusion equation as given in Eq. (3).

$$D\nabla^2\phi(\vec{r}, t) - \Sigma_a\phi(\vec{r}, t) + S(\vec{r}, t) = 0 \quad (3)$$

3.2. Neutron cross section

The probability of a particular reaction occurring between a neutron and a nucleus of an atom is called the microscopic cross section ($\sigma(E)$) of the nucleus for the particular reaction. This cross section varies with the energy of the neutron. The microscopic

absorption cross section decreases steadily with increasing neutron energy in a low energy region ($E < 1 eV$) (Lamarsh, 1966). Microscopic absorption and fission cross section of any nucleus can be obtained using these relations:

$$\sigma_a(E) = \frac{\sqrt{\pi}}{2} g_a(T) \left(\frac{T_0}{T}\right)^{\frac{1}{2}} \sigma(E_0) \quad (4)$$

and

$$\sigma_f(E) = \frac{\sqrt{\pi}}{2} g_f(T) \left(\frac{T_0}{T}\right)^{\frac{1}{2}} \sigma(E_0) \quad (5)$$

where, $\sigma_a(E)$ is the microscopic absorption cross section at higher temperature (> 20 °C), $\sigma_a(E_0)$ is the microscopic absorption cross section at the ambient temperature, $\sigma_f(E)$ is the microscopic fission cross section at higher temperature (> 20 °C), $\sigma_f(E_0)$ is the microscopic fission cross section at the ambient temperature, $g_f(T)$ is the non - $\frac{1}{v}$ fission factor and $g_a(T)$ is the non - $\frac{1}{v}$ absorption factor. T and T_0 are the absolute temperature and ambient temperature respectively of the neutron at

20 °C; where $T_0 = 273.15 + 20.46 = 293.61$ °K and $E_0 = 0.0253$ ev. However, the tendency of having a neutron interacting with a certain volume of nuclei depends not only on the microscopic cross section of the individual nuclei but also on the number of nuclei within that volume. Therefore, it is essential to define another kind of cross section termed as the macroscopic cross section (Σ). The macroscopic cross section is the probability of a given reaction occurring per unit travel of the neutron. Σ is related to the microscopic cross section ($\sigma(E)$) as follows:

$$\Sigma = N\sigma(E) \quad (6)$$

where Σ is the macroscopic cross section (cm^{-1}), $\sigma(E)$ is the microscopic cross section (cm^2) and N is the atom density of material ($atoms/cm^3$).

3.3. Solution to the steady state neutron diffusion equation and initial neutron flux calculation

The solution to the steady state neutron diffusion equation is obtained by employing the eigenfunction method. The central idea of the eigenfunction method is that it is possible to obtain

a solution to a diffusion equation in term of solutions of a differential equation (Lamarsh, 1966). The geometry of the reactor under study is cylindrical, the neutron source density is assumed to be distributed within the finite medium of the core in such a pattern that the diffusion equation is reduced to an ordinary differential equation (ODE). Therefore, from Eq. (3), we have

$$D\nabla^2\phi(r, z) - \Sigma_a\phi(r, z) = -S(r, z) . \tag{7}$$

$$\nabla^2 = \frac{1}{r} \frac{\partial}{\partial r} \left(r \frac{\partial}{\partial r} \right) + \frac{1}{r^2} \frac{\partial^2}{\partial \varphi^2} + \frac{\partial^2}{\partial z^2} . \tag{8}$$

$$\phi(r, z) = \frac{2S}{V\Sigma_a} \sum_{mn} \frac{1}{[B_{mn}^2 L^2 + 1] J_1^2(x_m)} J_0 \left(\frac{x_m r}{R_0} \right) \cos \left(\frac{n\pi z}{H} \right) . \tag{9}$$

$$B_{mn}^2 = \left(\frac{m\pi}{H} \right)^2 + \left(\frac{x_n}{R} \right)^2 . \tag{10}$$

where ∇^2 denotes the Laplacian operator for the cylindrical reactor as shown in Eq. (8). By applying all appropriate approximations and boundary conditions, Eq. (7) is solved to obtained Eq. (9) which is the complete solution to the neutron flux problem. where B_{mn}^2 is the reactor buckling and is expressed in Eq. (10).

pellet and water (H_2O) is considered. The reactor is assumed to be critical and operates at a power level of 25 Megawatts. The density of the fuel (UO_2) is 10.5 g/cm^3 with the ^{235}U enrichment of 20.5. Furthermore, the molecular weight and atom density of the fuel as well as the core buckling were computed and used in the initial neutron flux calculation.

However, in order to obtain the analytical solution for the initial neutron flux (i.e. flux at the start of a clean core), in this study, a finite cylindrical reactor core of radius 120 cm and height 300 cm consisting of a homogenous mixture of uranium dioxide (UO_2)

From Eq. (9), The fundamental neutron distribution function denoted by a constant A_{11} can be obtained from the power level P of the reactor (Lamarsh and Baratta, 2001).

$$A_{11} = \frac{2S}{V\Sigma_a[B_{11}^2 L^2 + 1] J_1^2(2.405)} = \frac{3.63 P}{V E_R \Sigma_f} . \tag{11}$$

$$A_{11} = \frac{3.63 P}{V E_R \Sigma_f} = 2.9875 \times 10^{13} \tag{12}$$

$$\Phi(r, z) = 2.9875 \times 10^{13} J_0 \left(\frac{x_m r}{R_0} \right) \cos \left(\frac{n\pi z}{H} \right) \tag{13}$$

$$\Phi(0,0) \equiv \Phi_0 = 2.9875 \times 10^{13} \text{ neutron/cm}^2\text{s} . \tag{14}$$

$$\Phi_T = \frac{2}{\sqrt{\pi}} \left(\frac{T}{T_0} \right)^{\frac{1}{2}} \Phi_0 , \tag{15}$$

From Eq. (11), E_R is the recoverable energy of the reactor, Σ_f is the macroscopic fission cross section

of the fuel, P is the reactor power and V is the volume of the reactor. Numerical evaluation of

constant A_{11} is obtained using some assumed values of a typical thermal reactor. Hence, Eq. (11) is solved and its value is shown in Eq. (12). Eq. (13) is obtained when Eq. (12) is substituted into Eq. (9). Hence, since the maximum value of the thermal neutron flux occurs at $r = 0$ and $z = 0$, the thermal neutron flux is obtained by explicitly solving Eq. (13) and its result is presented in Eq. (14).

In order to compute subsequent values of the thermal neutron flux at different temperatures, Eq. (15) was used to carry out the computation (Lamarsh, 2001), where Φ_0 is the initial thermal neutron flux obtained in Eq. (14), T_0 is the absolute temperature of the neutron and T is the ambient temperature of the neutron at 20 °C.

3.4. Solution to fission-product poisoning coupled rate equations

(i) Iodine -135

The iodine rate equation is:

$$\frac{\partial I(\vec{r},t)}{\partial t} = \gamma_I \bar{\Sigma}_f(\vec{r},t) \phi(\vec{r},t) - \lambda_I I(\vec{r},t), \quad (16)$$

$$e^{\lambda_I t} \frac{\partial I(\vec{r},t)}{\partial t} + \lambda_I I(\vec{r},t) e^{\lambda_I t} = \gamma_I \bar{\Sigma}_f(\vec{r},t) \phi(\vec{r},t) e^{\lambda_I t}, \quad (17)$$

$$\frac{\partial [I(\vec{r},t) e^{\lambda_I t}]}{\partial t} = \gamma_I \bar{\Sigma}_f(\vec{r},t) \phi(\vec{r},t) e^{\lambda_I t}, \quad (18)$$

$$\int_0^{\Delta t} dI(\vec{r},t) e^{\lambda_I t} dt = \gamma_I \bar{\Sigma}_f(\vec{r},0) \phi(\vec{r},0) \int_0^{\Delta t} e^{\lambda_I t} dt. \quad (19)$$

$$I(\vec{r},\Delta t) e^{\lambda_I \Delta t} - I(\vec{r},0) = \frac{\gamma_I}{\lambda_I} \bar{\Sigma}_f(\vec{r},0) \phi(\vec{r},0) [e^{\lambda_I \Delta t} - 1]. \quad (20)$$

$$I(\vec{r},\Delta t) e^{\lambda_I \Delta t} = \frac{\gamma_I}{\lambda_I} \bar{\Sigma}_f(\vec{r},0) \phi(\vec{r},0) [e^{\lambda_I \Delta t} - 1]. \quad (21)$$

$$I(\vec{r},\Delta t) = \frac{\gamma_I}{\lambda_I} \bar{\Sigma}_f(\vec{r},0) \phi(\vec{r},0) [1 - e^{-\lambda_I \Delta t}]. \quad (22)$$

$$e^{-\lambda_I \Delta t} = 1 - \frac{\lambda_I \Delta t}{1!} + \frac{(\lambda_I \Delta t)^2}{2!} - \frac{(\lambda_I \Delta t)^3}{3!}. \quad (23)$$

$$I(\vec{r},\Delta t) = \frac{\gamma_I}{\lambda_I} \bar{\Sigma}_f(\vec{r},0) \phi(\vec{r},0) [1 - (1 - \lambda_I \Delta t)]. \quad (24)$$

$$I(\vec{r},\Delta t) = \frac{\gamma_I}{\lambda_I} \bar{\Sigma}_f(\vec{r},0) \phi(\vec{r},0) [\lambda_I \Delta t]. \quad (25)$$

$$\int_t^{t+\Delta t} \partial I(\vec{r},t) e^{\lambda_I t} = \gamma_I \bar{\Sigma}_f(\vec{r},t) \phi(\vec{r},t) \int_t^{t+\Delta t} e^{\lambda_I t} dt. \quad (26)$$

Equation (16) is the buildup and burn up rate equation for Iodine-135 where I is the number of ^{135}I atoms/cm³ i.e. the atom density of iodine, γ_I is

This section presents the buildup and burnup rate equations for Xenon-135, its precursor Iodine-135 and Samarium-149 as well as its precursor-Promethium-149. These production-destruction rate equations distinctively depicts how the individual fission isotopes are formed and how they dissappeared. The analytical solution to the coupled rate equations were equally presented.

3.4.1. Derivation of Xenon-135 rate equation

Xenon-135 is produced in the reactor fuel in two ways (Lamarsh, (2001):

- a) Directly from fission. About 0.3% of all fission products are Xenon-135.
- b) Indirectly from the decay of Iodine-135, this is either produced as a fission product or from the decay of the fission product Tellurium-135.

the effective yield of the isotope, and $\bar{\Sigma}_f$ is the average thermal fission cross section.

Multiplying both sides of Eq. (16) by the integration factor; $e^{\lambda_I t}$, we have Eq. (17). By simplifying Eq. (17), Eq. (18) is obtained.

However, assuming we are dealing with a “clean core” at the start of the reactor, the concentration of iodine-135 isotope is zero at $t = 0$ and the neutron flux in the reactor is assumed to be constant in the interval $0 < t < \Delta t$, by applying this approximation to Eq. (18), we obtained Eq. (19). By carrying out the Integration on Eq. (19) over the limit $0 \rightarrow \Delta t$, we have Eq. (20). Since the reactor core is assumed

to be clean within this time interval where $I(\vec{r}, 0) = 0$, therefore, Eq. (20) results to Eq. (21). By multiplying both sides of Eq. (21) by $e^{-\lambda_I \Delta t}$, Eq. (22) is obtained.

In a bid to simplify Eq. (22), we must apply Taylor’s expansion approximation stated in Eq. (23), hence, we obtain Eq. (24). with further simplification of Eq. (24), we have Eq. (25). However, it is very important to derive a more general solution for ^{135}I concentration at $t + \Delta t$, in terms of its concentration at time t . Applying the constant flux approximation to Eq. (18), we have Eq. (26).

$$I(\vec{r}, t + \Delta t)e^{\lambda_I(t+\Delta t)} - I(\vec{r}, t)e^{\lambda_I t} = \frac{\gamma_I}{\lambda_I} \bar{\Sigma}_f(\vec{r}, t)\phi(\vec{r}, t) [e^{\lambda_I(t+\Delta t)} - e^{\lambda_I t}]. \quad (27)$$

$$I(\vec{r}, t + \Delta t) = I(\vec{r}, t)e^{-\lambda_I \Delta t} + \frac{\gamma_I}{\lambda_I} \bar{\Sigma}_f(\vec{r}, t)\phi(\vec{r}, t)[1 - e^{-\lambda_I \Delta t}]. \quad (28)$$

$$I(\vec{r}, t + \Delta t) = I(\vec{r}, t)[1 - \lambda_I \Delta t] + \frac{\gamma_I}{\lambda_I} \bar{\Sigma}_f(\vec{r}, t)\phi(\vec{r}, t)[\lambda_I \Delta t]. \quad (29)$$

By re-arranging Eq. (27) and multiplying both sides by $e^{-\lambda_I(t+\Delta t)}$, we obtain Eq. (28). Introducing Taylor’s expansion approximation into Eq. (28), the

general solution for ^{135}I concentration at $t + \Delta t$, in terms of its concentration at time t is thus presented in Eq. (29).

(ii) **Xenon-135**

The xenon rate equation is:

$$\frac{\partial X_e(r,t)}{\partial t} = \lambda_I I(\vec{r}, t) + \gamma_X \Sigma_f(\vec{r}, t)\phi(\vec{r}, t) - \lambda_X X(\vec{r}, t) - \sigma_{ax} X(\vec{r}, t)\phi(\vec{r}, t). \quad (30)$$

$$\lambda_I I(\vec{r}, t) + \gamma_X \Sigma_f(\vec{r}, t)\phi(\vec{r}, t) - \lambda_X X(\vec{r}, t) - \sigma_{ax} X(\vec{r}, t)\phi(\vec{r}, t) = 0. \quad (31)$$

$$\lambda_I I(\vec{r}, t) + \gamma_X \Sigma_f(\vec{r}, t)\phi(\vec{r}, t) = \lambda_X X(\vec{r}, t) - \sigma_{ax} X(\vec{r}, t)\phi(\vec{r}, t). \quad (32)$$

$$\lambda_I I(\vec{r}, t) + \gamma_X \Sigma_f(\vec{r}, t)\phi(\vec{r}, t) [\lambda_X - \sigma_{ax}\phi(\vec{r}, t)] X(\vec{r}, t) \quad (33)$$

$$X(\vec{r}, t) = \frac{\lambda_I I(\vec{r}, t) + \gamma_X \Sigma_f(\vec{r}, t)\phi(\vec{r}, t)}{\lambda_X + \sigma_{ax}\phi(\vec{r}, t)}. \quad (34)$$

$$\frac{\partial I(\vec{r}, t)}{\partial t} = \gamma_I \Sigma_f(\vec{r}, t)\phi(\vec{r}, t) - \lambda_I I(\vec{r}, t), \quad (35)$$

$$\frac{\partial I(\vec{r}, t)}{\partial t} = 0. \quad (36)$$

$$\lambda_I I(\vec{r}, t) = \gamma_I \Sigma_f(\vec{r}, t)\phi(\vec{r}, t). \quad (37)$$

$$I(\vec{r}, t) = \frac{\gamma_X \Sigma_f(\vec{r}, t) \phi(\vec{r}, t)}{\lambda_I} \quad (38)$$

$$X(\vec{r}, t)_\infty = \frac{\gamma_I \Sigma_f(\vec{r}, t) \phi(\vec{r}, t) + \gamma_X \Sigma_f(\vec{r}, t) \phi(\vec{r}, t)}{\lambda_X + \sigma_{aX} \phi(\vec{r}, t)} \quad (39)$$

Since the half-lives of I-135 and Xe-135 are so short and the absorption cross-section of the xenon-135 isotope is so large, the concentration of these isotopes quickly rise to saturation or equilibrium values. This concentration can be formed by placing the time derivative in Eq. (16) and Eq. (30) equal to zero, (Lamarsh, 2001). Therefore, by evaluating

these two (2) equations carefully, Eq. (30) is translated into Eq. (34) and Eq. (16) into Eq. (38) respectively. By substituting Eq. (38) into Eq. (34), we obtain Eq. (39) which is the equation for equilibrium xenon.

$$\frac{\partial X(\vec{r}, t)}{\partial t} + \lambda_X X(\vec{r}, t) + \overline{\sigma_{aX}} \phi(\vec{r}, t) X(\vec{r}, t) = \lambda_I I(\vec{r}, t) + \gamma_X \overline{\Sigma_f}(\vec{r}, t) \phi(\vec{r}, t), \quad (40)$$

$$\frac{\partial X(\vec{r}, t)}{\partial t} + [\lambda_X + \overline{\sigma_{aX}} \phi(\vec{r}, t)] X(\vec{r}, t) = \lambda_I I(\vec{r}, t) + \gamma_X \overline{\Sigma_f}(\vec{r}, t) \phi(\vec{r}, t). \quad (41)$$

$$e^{[\lambda_X + \overline{\sigma_{aX}} \phi(\vec{r}, t)] t} \frac{\partial X(\vec{r}, t)}{\partial t} + [\lambda_X + \overline{\sigma_{aX}} \phi(\vec{r}, t)] X(\vec{r}, t) e^{[\lambda_X + \overline{\sigma_{aX}} \phi(\vec{r}, t)] t} = \lambda_I I(\vec{r}, t) e^{[\lambda_X + \overline{\sigma_{aX}} \phi(\vec{r}, t)] t} + \gamma_X \overline{\Sigma_f}(\vec{r}, t) \phi(\vec{r}, t) e^{[\lambda_X + \overline{\sigma_{aX}} \phi(\vec{r}, t)] t}. \quad (42)$$

$$\frac{\partial [X(\vec{r}, t) e^{[\lambda_X + \overline{\sigma_{aX}} \phi(\vec{r}, t)] t}]}{\partial t} = \lambda_I I(\vec{r}, t) e^{[\lambda_X + \overline{\sigma_{aX}} \phi(\vec{r}, t)] t} + \gamma_X \overline{\Sigma_f}(\vec{r}, t) \phi(\vec{r}, t) e^{[\lambda_X + \overline{\sigma_{aX}} \phi(\vec{r}, t)] t}. \quad (43)$$

$$\int_0^{\Delta t} \partial [X(\vec{r}, t) e^{[\lambda_X + \overline{\sigma_{aX}} \phi(\vec{r}, t)] t}] dt = \lambda_I I(\vec{r}, 0) \int_0^{\Delta t} e^{[\lambda_X + \overline{\sigma_{aX}} \phi(\vec{r}, 0)] t} dt + \gamma_X \overline{\Sigma_f}(\vec{r}, 0) \phi(\vec{r}, 0) \int_0^{\Delta t} e^{[\lambda_X + \overline{\sigma_{aX}} \phi(\vec{r}, 0)] t} dt. \quad (44)$$

$$X(\vec{r}, \Delta t) e^{[\lambda_X + \overline{\sigma_{aX}} \phi(\vec{r}, 0)] \Delta t} = \frac{\lambda_I I(\vec{r}, 0)}{\lambda_X + \sigma_{aX} \phi(\vec{r}, 0)} [e^{[\lambda_X + \overline{\sigma_{aX}} \phi(\vec{r}, 0)] \Delta t} - 1] + \frac{\gamma_X \overline{\Sigma_f}(\vec{r}, 0) \phi(\vec{r}, 0)}{\lambda_X + \sigma_{aX} \phi(\vec{r}, 0)} [e^{[\lambda_X + \overline{\sigma_{aX}} \phi(\vec{r}, 0)] \Delta t} - 1]. \quad (45)$$

$$X(\vec{r}, \Delta t) e^{[\lambda_X + \overline{\sigma_{aX}} \phi(\vec{r}, 0)] \Delta t} = \left[\frac{\lambda_I I(\vec{r}, 0)}{\lambda_X + \sigma_{aX} \phi(\vec{r}, 0)} + \frac{\gamma_X \overline{\Sigma_f}(\vec{r}, 0) \phi(\vec{r}, 0)}{\lambda_X + \sigma_{aX} \phi(\vec{r}, 0)} \right] [e^{[\lambda_X + \overline{\sigma_{aX}} \phi(\vec{r}, 0)] \Delta t} - 1], \quad (46)$$

$$X(\vec{r}, \Delta t) e^{[\lambda_X + \overline{\sigma_{aX}} \phi(\vec{r}, 0)] \Delta t} = \left[\frac{\lambda_I I(\vec{r}, 0) + \gamma_X \overline{\Sigma_f}(\vec{r}, 0) \phi(\vec{r}, 0)}{\lambda_X + \sigma_{aX} \phi(\vec{r}, 0)} \right] [e^{[\lambda_X + \overline{\sigma_{aX}} \phi(\vec{r}, 0)] \Delta t} - 1]. \quad (47)$$

$$X(\vec{r}, \Delta t) = \left[\frac{\lambda_I I(\vec{r}, 0) + \gamma_X \overline{\Sigma_f}(\vec{r}, 0) \phi(\vec{r}, 0)}{\lambda_X + \sigma_{aX} \phi(\vec{r}, 0)} \right] [1 - e^{-[\lambda_X + \overline{\sigma_{aX}} \phi(\vec{r}, 0)] \Delta t}], \quad (48)$$

$$I(\vec{r}, 0) = \frac{\gamma_I \overline{\Sigma_f}(\vec{r}, 0) \phi(\vec{r}, 0)}{\lambda_I}. \quad (49)$$

$$X(\vec{r}, \Delta t) = \left[\frac{\gamma_I \overline{\Sigma_f}(\vec{r}, 0) \phi(\vec{r}, 0) + \gamma_X \overline{\Sigma_f}(\vec{r}, 0) \phi(\vec{r}, 0)}{\lambda_X + \sigma_{aX} \phi(\vec{r}, 0)} \right] [1 - e^{-[\lambda_X + \overline{\sigma_{aX}} \phi(\vec{r}, 0)] \Delta t}]. \quad (50)$$

$$X(\vec{r}, \Delta t) = \left[\frac{[\gamma_I + \gamma_X] \overline{\Sigma_f}(\vec{r}, 0) \phi(\vec{r}, 0)}{\lambda_X + \sigma_{aX} \phi(\vec{r}, 0)} \right] [1 - e^{-[\lambda_X + \overline{\sigma_{aX}} \phi(\vec{r}, 0)] \Delta t}]. \quad (51)$$

$$\int_t^{t+\Delta t} \partial X(\vec{r}, t) e^{[\lambda_X + \overline{\sigma_{aX}}\phi(\vec{r}, t)]t} dt = \int_t^{t+\Delta t} \lambda_I I(\vec{r}, t) e^{[\lambda_X + \overline{\sigma_{aX}}\phi(\vec{r}, t)]t} dt + \int_t^{t+\Delta t} \gamma_X \overline{\Sigma_f}(\vec{r}, t) \phi(\vec{r}, t) e^{[\lambda_X + \overline{\sigma_{aX}}\phi(\vec{r}, t)]t} dt, \tag{52}$$

$$\int_t^{t+\Delta t} \partial X(\vec{r}, t) e^{[\lambda_X + \overline{\sigma_{aX}}\phi(\vec{r}, t)]t} dt = \lambda_I I(\vec{r}, t) \int_t^{t+\Delta t} e^{[\lambda_X + \overline{\sigma_{aX}}\phi(\vec{r}, t)]t} dt + \gamma_X \overline{\Sigma_f}(\vec{r}, t) \phi(\vec{r}, t) \int_t^{t+\Delta t} e^{[\lambda_X + \overline{\sigma_{aX}}\phi(\vec{r}, t)]t} dt. \tag{53}$$

$$X(\vec{r}, t + \Delta t) e^{[\lambda_X + \overline{\sigma_{aX}}\phi(\vec{r}, t)]t+\Delta t} = X(\vec{r}, t) e^{[\lambda_X + \overline{\sigma_{aX}}\phi(\vec{r}, t)]t} + \frac{[\lambda_I I(\vec{r}, t) + \gamma_X \overline{\Sigma_f}(\vec{r}, t) \phi(\vec{r}, t)]}{\lambda_X + \overline{\sigma_{aX}}\phi(\vec{r}, t)} [e^{[\lambda_X + \overline{\sigma_{aX}}\phi(\vec{r}, t)]t+\Delta t} - e^{[\lambda_X + \overline{\sigma_{aX}}\phi(\vec{r}, t)]t}]. \tag{54}$$

$$X(\vec{r}, t + \Delta t) = X(\vec{r}, t) e^{-[\lambda_X + \overline{\sigma_{aX}}\phi(\vec{r}, t)]\Delta t} + \frac{[\lambda_I I(\vec{r}, t) + \gamma_X \overline{\Sigma_f}(\vec{r}, t) \phi(\vec{r}, \Delta t)]}{\lambda_X + \overline{\sigma_{aX}}\phi(\vec{r}, 0)} [1 - e^{-[\lambda_X + \overline{\sigma_{aX}}\phi(\vec{r}, t)]\Delta t}]. \tag{55}$$

$$e^{-[\lambda_X + \overline{\sigma_{aX}}\phi(\vec{r}, t)]t} = 1 - \frac{[\lambda_X + \overline{\sigma_{aX}}\phi(\vec{r}, t)]t}{1!} + \frac{[\lambda_X + \overline{\sigma_{aX}}\phi(\vec{r}, t)]t^2}{2!} - \dots \tag{56}$$

$$X(\vec{r}, t + \Delta t) = X(\vec{r}, t) \{1 - [\lambda_X + \overline{\sigma_{aX}}\phi(\vec{r}, t)]\Delta t\} + \frac{[\lambda_I I(\vec{r}, t) + \gamma_X \overline{\Sigma_f}(\vec{r}, t) \phi(\vec{r}, t)]}{\lambda_X + \overline{\sigma_{aX}}\phi(\vec{r}, 0)} [[\lambda_X + \overline{\sigma_{aX}}\phi(\vec{r}, t)]\Delta t]. \tag{57}$$

By rearranging Eq. (40), we have Eq. (41). Eq. (42) is obtained by multiplying both sides of Eq. (41) by the integration factor $e^{[\lambda_X + \overline{\sigma_{aX}}\phi(\vec{r}, t)]t}$. This resulted into Eq. (43). Eq. (43) is further simplified extensively to obtain the atom concentration of Xe-135 just shortly after the reactor’s startup (within the time interval $0 \rightarrow \Delta t$) and this is expressed in Eq. (51). Moreover, as in the case of Iodine-135 atom concentration, in order to obtain the general solution of ^{135}Xe at $(t + \Delta t)$ in terms of its concentration at t , by applying all appropriate boundary conditions and approximations to Eq. (43), we have Eq. (57). Hence, Eq. (57) represents the atom concentration of ^{135}Xe at $(t + \Delta t)$ in terms of its concentration at t and therefore is used for the

numerical computation of xenon-135 atom concentration at subsequent time intervals.

3.4.2. Derivation of Samarium-149 rate equation

Samarium-149 is the most important of the stable fission products. It is formed in the fuel by the decay of fission products Neodymium-149 and Promethium-149 (Stacey, 2007).

Consequently, by adopting similar mathematical methods used in solving for the above Iodine-135 rate equations above (i.e. Eq. 16). The general solution to Pm-149 and Sm-149 concentration at $(t + \Delta t)$, in terms of its concentration at time t , are expressed respectively:

$$P(\vec{r}, t + \Delta t) = P(\vec{r}, \Delta t)[1 - \lambda_P t] + \frac{\gamma_P}{\lambda_P} \overline{\Sigma_f}(\vec{r}, \Delta t) \phi(\vec{r}, \Delta t) [\lambda_P t]. \tag{58}$$

and

$$S(\vec{r}, t + \Delta t) = S(\vec{r}, t)(1 - \sigma_{aS}\phi(\vec{r}, t)t) - \frac{\lambda_P P(\vec{r}, t)}{\sigma_{aS}\phi(\vec{r}, t)} [\sigma_{aS}\phi(\vec{r}, t)t]. \tag{59}$$

3.4.3. Nuclide burn-up time

The various time steps during which the fission nuclides concentrations were observed to buildup and burnup is calculated with the aid of nuclide burn-up time equation. The burnup time for any nuclide is the time necessary to transmuted by

neutron absorption to half of the quantity of a nuclide under neutron irradiation (Berthou *et al.*, 2003). It also refers to the disappearance of an isotope. The time evolution of a quantity N of an isotope under neutron irradiation is given by:

$$\frac{\partial N}{\partial t} = -(\lambda + \sigma\phi)N, \quad (60)$$

where ϕ is the flux, σ the absorption cross-section, and λ the decay constant.

$$\frac{\partial N}{N} = -(\lambda + \sigma\phi)dt. \quad (61)$$

Applying integration to both sides of Eq. (61)

$$\ln \left[\frac{N(t)}{N_0} \right] = -(\lambda + \sigma\phi)t, \quad (62)$$

$$\frac{N(t)}{N_0} = e^{-(\lambda + \sigma\phi)t}, \quad (63)$$

and

$$N(t) = N_0 e^{-(\lambda + \sigma\phi)t}. \quad (64)$$

Hence, for the selected nuclei, the individual nuclide burnout time is given by:

$$\tau_{BU} = \frac{\ln 2}{(\lambda + \sigma\phi)}. \quad (65)$$

where τ_{BU} is the burnout time of the isotope.

3.4.4. JaC-FPBB code flow chart

Figure 3.1 shows the flow chart for JaC-FPBB Code (algorithm). In Figure 3.1, we show the calculated ambient temperature T_n in degree kelvin for seven different temperature levels. The temperatures

obtained are then used to compute new neutron energies and fluxes. The calculated new neutron energies as well as fluxes and values of other constants were used to calculate the fission product atom concentrations.

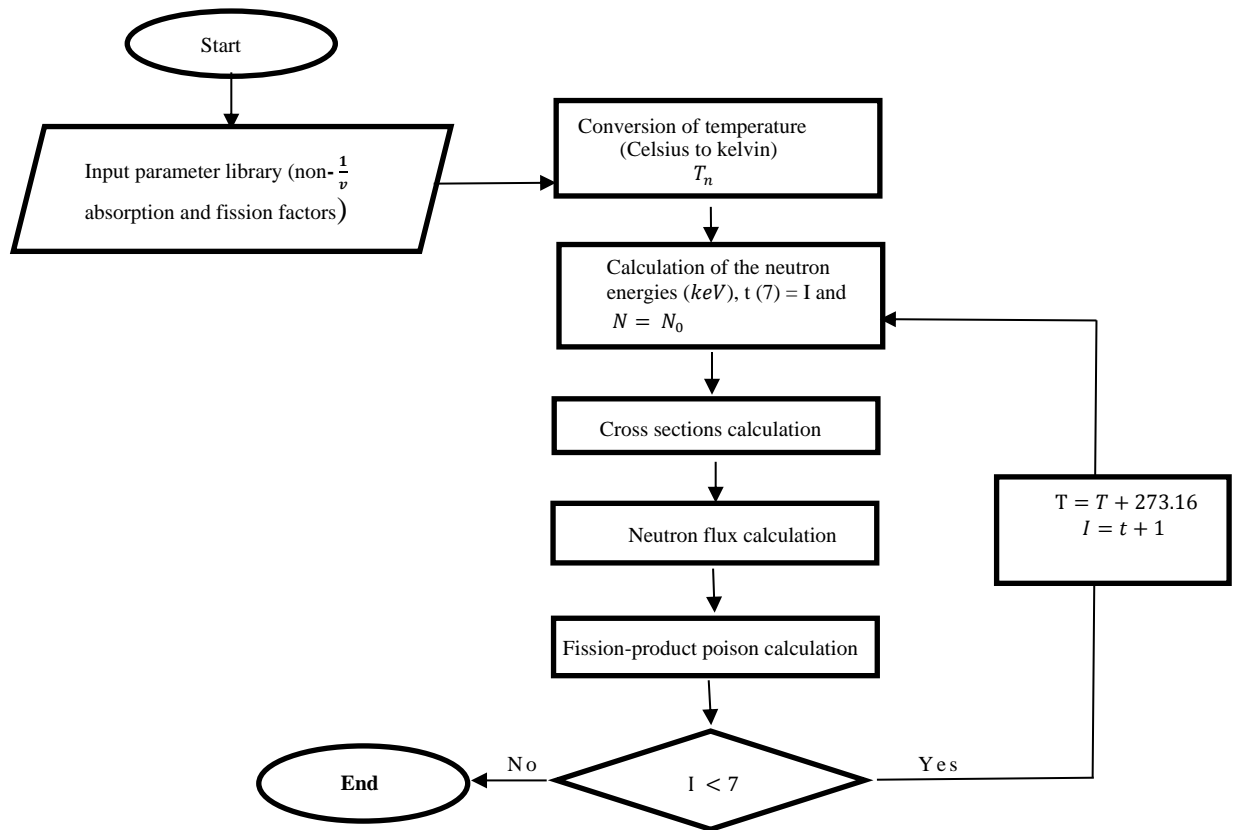


Figure 3.1. Flow chart for the Jac-FPBB code.

4. Result and Discussion

This section presents the atom concentrations of the two vital fission product poisons relevant to this study (Xenon-135 and Samarium-149) when the program JaC-FPBB code is run. The temperature variations of the neutron flux and neutron energy in the reactor core as well as the computed cross-sections for, Xenon-135 and Samarium-149 needed for their respective atom concentration computations were also presented. The atom concentrations at only seven (7) different burnup times were conducted because the fluxes at temperatures higher than 1000 °C could not be calculated due to lack of nuclear data from available literatures.

4.1. Temperature variation of neutron flux and neutron energy

Having obtained the initial thermal neutron flux Φ_0 from Eq. (14), the thermal neutron flux $\Phi_T(E)$ at different available energies were calculated using the relationship between Φ_T and Φ_0 from Eq. (15). Table 4.1 shows the temperature variation values of

neutron fluxes and neutron energies. From the Table 4.1, it is observed that the values of the neutron flux increases as the temperature of the fuel and the corresponding energy increase. The thermal neutron fluxes obtained were used in computing the atom concentrations of the fission products poison.

4.2. Computed cross-sections for poison fission-products

The average microscopic and macroscopic absorption and fission cross-sections for Iodine-135, Xenon-135, Promethium-149 and Samarium-149 were computed using Eq. (4), Eq. (5) and Eq. (6) but, only the values obtained for Xenon-135 and Samarium-149 are presented in Table 4.2 and Table 4.3 respectively. It was observed from Table 4.2 and 4.3 that the computed cross-sections decrease with increasing fuel temperature. This is expected since the microscopic absorption and fission cross sections of the fissile material used (Uranium-235) are inversely proportional to the temperature of the fuel. These computed cross-sections were used to calculate the atom concentrations of Xenon-135 and Samarium-149.

Table 4.1. Temperature variation of neutron energies and fluxes.

Temperature (°C)	Neutron Energy (KeV)	Neutron Flux $\Phi_T(E)$
20	0.0253	2.7219x10 ¹³
100	0.0322	3.0709x10 ¹³
200	0.0408	3.4580x10 ¹³
400	0.0580	4.1245x10 ¹³
600	0.0752	4.6975x10 ¹³
800	0.0925	5.2077x10 ¹³
1000	0.1097	5.6723x10 ¹³

Table 4.2. Computed cross-sections for Xenon-135.

T ⁰ c	$\bar{\sigma}_{aXe}$ (barn)	$\bar{\Sigma}_{aXe}$ (cm ⁻¹)
20	5.54x10 ⁻⁶	47197.65
100	5.13x10 ⁻⁶	43719.20
200	4.66x10 ⁻⁶	39649.82
400	3.75x10 ⁻⁶	31907.93
600	3.03x10 ⁻⁶	25772.93
800	2.47x10 ⁻⁶	21060.03
1000	2.03x10 ⁻⁶	17322.91

Table 4.3. Computed cross-sections for Samarium-149.

T^0c	$\bar{\sigma}_{as}$ (barn)	$\bar{\Sigma}_{as}$ (cm^{-1})
20	1.17×10^{-5}	1144.80
100	1.21×10^{-5}	1184.37
200	1.19×10^{-5}	1164.86
400	1.04×10^{-5}	1021.04
600	8.74×10^{-4}	855.40
800	7.24×10^{-4}	712.16
1000	6.10×10^{-4}	596.83

4.3. Graphical representation of time variation of Xenon-135 concentration

Figure 4.2 shows the plot of atom concentration of Xenon-135 isotope against time. At the origin of time (at $t = 0$), the concentration of Xenon-135 is zero, which signified that the reactor was clean and free of poison before it is being put to use. Three segments of the plot are considered in the following time intervals: 0-17 hours, 17-18 hours and 18-21 hours. At the time interval 0-17 hours the concentration of Xenon-135 buildup linearly from 6.96×10^{13} atoms/cm³ to 3.83×10^{14} atoms/cm³. This buildup was mainly due to contributions from both

fission of Uranium-235 and decay of Iodine-135 ($T_{1/2}$ of Iodine-135 is 6.6 hours) at this stage. within the time interval 17-18 hours, the concentration of Xenon-135 isotope shown in the profile depicts a little deviation from the original linear shape. This marks the starting point for Xenon-135 buildup from fission of Uranium-235 and decay of Iodine-135 equals its disappearance due to neutron absorption to form Xenon-136 and beta decay to form Cesium-135. Shortly after this time interval, i.e. between 18 hours to approximately 21 hours of the simulation, the equilibrium buildup of Xenon-135 begins to surface.

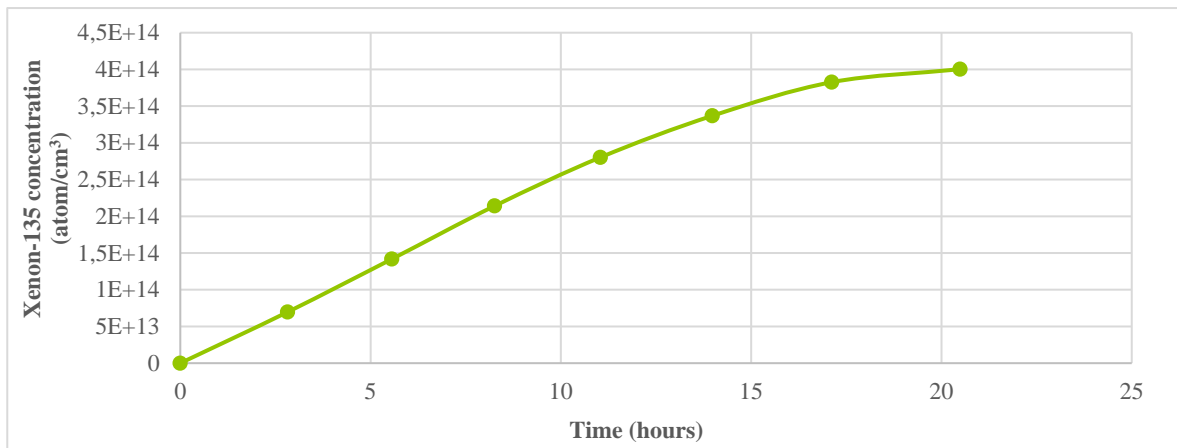


Figure 4.2. Plot of Xenon-135 concentration against time.

4.4. Graphical representation of time variation of Samarium-149 concentration

Figure 4.4 shows the profile of Samarium-149 concentration against time in an operating reactor that startup from a clean core. At the initial time of the analysis (at $t = 0$) the concentration of Samarium-149 was zero. This validates one of the assumptions made that at the start of the reactor the concentration of all poisons were zero. From time 0-510 hours the concentration of Samarium-149

increases linearly to 5.3×10^{16} atom/cm³ own to its production from the decay of Promethium-149 and removal solely by neutron absorption to produce to Samarium-150 isotope. As shown by the Samarium-149 profile, at exactly 510 hours of this simulation, equilibrium Samarium-149 began to form till 605 hours of the simulation. It should be noted that, the long duration taken to simulate Samarium-149 concentration is as a result of its lone production from the decay of Promethium-149 which have a half-life of 54 hours. By implication,

this means that Samarium-149 is expected to begin its significant buildup after 54 hours of Promethium-149 formation.

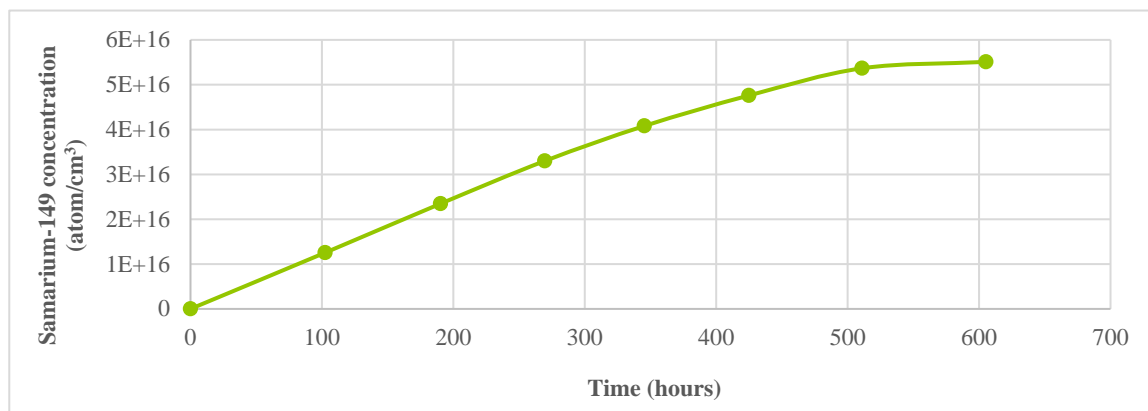


Figure 4.4. Plot of Samarium-149 concentration against time.

5. Conclusion

In this paper, four important fission products were investigated which includes: Iodine-135, Xenon-135, Promethium-149 and Samarium-149 but with special focus and consideration on Xenon-135 and Samarium-149 because of their large absorption cross sections. The result from JaC-FPBB computed the temperature variations of neutron energies and fluxes, the fission isotopes microscopic and macroscopic cross sections and most importantly, the fission-product poisoning atom concentrations within a computed time. In this study, the result obtained show that it takes Xenon-135 and Samarium-149, 17 hours and 510 hours respectively to buildup and attain equilibrium. The discrepancy between the two fission nuclide's equilibrium attainment time is not far fetch. Since, there is no direct production of Samarium-149 from fission as with Xenon-135; aside from beta decay of Promethium-149 which has a considerable long half-life coupled with the fact that Samarium-149 has a much lower cross section (4.2×10^6 barn) than Xenon-135, Consequentially, it will correspondingly take longer time for Samarium-149 to attain equilibrium than Xenon-135 as shown in this study. This study concluded that the designed algorithm (JaC-FPBB code) proved efficient as it could compute the build-up and burn-up rates for

the two important fission fragments in a nuclear reactor core. The code is easily accessible and could serve as a tool for the development of nuclear energy in developing countries, especially Nigeria.

Acknowledgements

Authors wish to acknowledge the support provided by the Department of Physics and Engineering Physics, the Center for Energy Research and Development and the Department of Electronic and Electrical Engineering, Obafemi Awolowo University, Ile-Ife, Osun State, Nigeria.

References

- Arshad, M. (1994). Study Of Xenon And Samarium behaviour in the LEU Parr-1 Cores. Pakistan: Nuclear Engineering Division, Pakistan Institute of Nuclear Science & Technology, 4(28), pp. 1-21.
- Briesmeister, J. F. (1993). MCNP - A General Monte Carlo N-Particle Transport Code, Los Alamos National Laboratory, New Mexico, USA, pp. 4-12.
- Berthou, V., Degueudre, C., Magill, J. (2003). Transmutation Characteristics in Thermal and Fast Neutron Spectra: Application to Americium, Journal of Nuclear Materials, pp. 156-162.

- England, T.R., Wilson. W.B., Stamatelatos, M.G. (1976). Fission product data for thermal reactors- A data set for EPRI-CINDER using ENDF/B-IV. USA: Los Alamos Scientific Laboratory, 8(9), 81p.
- Fermi, E. (1940). Nuclear disintegrations, In: Electrical Engineering, 59(2), pp. 57-58.
- Hermann, O. W., Wesfall, R. M. (1998). ORIGEN-S: Scale System Module to Calculated Fuel Depletion Actinide Transmutation, Fission Product Build-up, Decay and Associated Radiation Source Terms. Tennessee, USA: Oak Ridge National Laboratory, 6(2), pp. 1-122.
- Marcum, W., Spinrad, B. I. (2013). Nuclear reactor device, pp. 1-8. [Online]. Available: www.britannica.com/technology/nuclear-reactor.
- Kord, S., Lulu, L. (2012). Nuclear Reactor Physics, Massachusetts Institute of Technology, 372p.
- Lamarsh, J. R. (1966). Introduction to Nuclear Reactor Theory. New york: Addison-Wesley Publishing Company, pp. 255-256.
- Lamarsh, J. R. (2001). Introduction to Nuclear Reactor Theory. New york: Addison-Wesley Publishing Company, 501p.
- Lamarsh, J. R, Baratta, A. J. (2001). Introduction to Nuclear Engineering. Newjersy: Prentice-Hall, Inc. Publishing Company, 3, pp. 272-281.
- Parma, E. J. (2002). BURNCAL- A Nuclear Reactor Burnup Code Using MCNP Tallies. California: Sandia National Laboratories, pp. 3-102.
- Stacey, W. M. (2007). Nuclear Reactor Physics, New york: Wiley-VCH Publishing Company, 2, pp. 211-215.
- Yesilyurt, G., Clarno, K. T., Gauld, I. C. (2011). Modular Origen-S for Multi-Physics Code Systems. International Conference on Mathematics and Computational Methods Applied to Nuclear Science and Engineering, Rio de Janeiro, Brazil, pp. 1-14.